Formation and interaction of multiple coherent phase space structures in plasma

Amar Kakad,[1,a)] Bharati Kakad,[1,b)] and Yoshiharu Omura[2,c)]

[1]*Indian Institute of Geomagnetism, New Panvel, Navi Mumbai 410-218, India*
[2]*Research Institute for Sustainable Humanosphere, Kyoto University, Uji, Kyoto 611-0011, Japan*

The head-on collision of multiple counter-propagating coherent phase space structures associated with the ion acoustic solitary waves (IASWs) in plasmas composed of hot electrons and cold ions is studied here by using one-dimensional Particle-in-Cell simulation. The chains of counter-propagating IASWs are generated in the plasma by injecting the Gaussian perturbations in the equilibrium electron and ion densities. The head-on collisions of the counter-propagating electron and ion phase space structures associated with IASWs are allowed by considering the periodic boundary condition in the simulation. Our simulation shows that the phase space structures are less significantly affected by their collision with each other. They emerge out from each other by retaining their characteristics, so that they follow soliton type behavior. We also find that the electrons trapped within these IASW potentials are accelerated, while the ions are decelerated during the course of their collisions. *Published by AIP Publishing.* [http://dx.doi.org/10.1063/1.4986109]

A number of spacecraft[1–5] and experimental[6–9] observations have well established the existence of nonlinear solitary wave structures in various plasma environments.[10,11] The criterion for a solitary wave to be identified as a soliton is that, it has to survive a collision (head-on or overtaking) with another solitary wave. Therefore, understanding the particle and wave dynamical processes at the interaction region is important to investigate the physics of the wave-wave interaction phenomenon. It is extremely difficult to track such a process in space plasma environments with the help of spacecraft, as it required multiple spacecraft at appropriate positions in the propagation path of the interacting waves. Consequently, computer simulation is the suitable technique to investigate the evolutionary dynamics of such a process.

The problem of the head-on collision of the solitary waves in different plasmas has been addressed by numerous theoretical and experimental studies.[12–25] These studies have used different approaches viz. theory,[16,17,19,26] numerical simulations,[15,21,25] and laboratory experiments[14] to deal with the dynamical behaviour of solitary waves after their head-on collision. Among these, most of the studies are based on the fluid approach, which employed extension of the Poincare-Lighthill-Kuo (PLK) method of strained coordinates to investigate the phase shifts and the trajectories after the head-on collision of the two counter propagating solitary wave structures.

Among the solitary waves, the ion acoustic solitary waves (IASWs) are the most basic modes supported by the simplest form of multi-species plasmas. The collision of two IASWs in plasmas composed of hot electrons and cold ions has been studied by using the PLK perturbation method and one-dimensional Particle-in-Cell (PIC) simulation.[15] However, the

objective of their work was to compare the results from the PLK method with the PIC simulations. The present study is carried out with a different motivation. Here, we have not only examined the dynamical characteristics of the IASWs after their head-on collision with the multiple IASW structures, but also investigated the local particle dynamics during such interactions. To address these issues, we carry out one-dimensional PIC simulations for one of the plasma models that supports the formation of multiple IASW structures. We have used a one-dimensional electromagnetic PIC code based on the Kyoto university ElectroMagnetic Particle Code (KEMPO).[6,27,28] In this code, Maxwell's equations and equations of motion are solved for a large number of superparticles.[29] Both spatial and time derivatives in the equations are solved by the centered finite difference scheme. We assume two species, electrons and ions (H^+), in the simulation system with the periodic boundary conditions. The initial velocity distributions of electrons and ions are assumed to be shifted-Maxwellian distributions given by

$$f_j(v) = \frac{n_j}{\sqrt{2\pi}\, V_{t\|j}} \exp\left(-\frac{\left(v - V_{d\|j}\right)^2}{2V_{t\|j}^2}\right), \qquad (1)$$

where the subscripts $j = e$, i represent the electrons and ions, respectively. The parameters $V_{t\|j}$, $V_{d\|j}$, and n_j represent the thermal velocity and drift velocity parallel to the magnetic field and number density for species j, respectively. The parameters for the simulation run are grid spacing $\Delta x = 1$, time interval $\Delta t = 0.002$, system length $L_x = 4000$, ion to electron mass ratio $m_i/m_e = 100$, thermal velocities $V_{t\|e} = 70$ and $V_{t\|i} = 0.5$, drift velocities $V_{d\|e} = V_{d\|i} = 0$, and plasma frequencies $\omega_{pe} = 10$. The values of $V_{t\|e}$ and $V_{t\|i}$ imply that $T_e = 49$ and $T_i = 0.25$. The ion Debye length and plasma frequency are $\lambda_{di} = 0.5$ and $\omega_{pi} = 1$, respectively. We perturbed the equilibrium electron and ion densities with the standard Gaussian perturbation in electron and ion equilibrium

a)amar@iigs.iigm.res.in
b)ebharati@iigs.iigm.res.in
c)omura@rish.kyoto-u.ac.jp

densities. Therefore, the superparticles in the simulation are distributed by using the following equation:

$$n_j(x) = n_{j0} + \Delta n \exp\left(-\frac{(x - x_c + \alpha)^2}{l_0^2}\right). \qquad (2)$$

In the equation above, n_{j0} is the equilibrium density of the species j. Here, $j = e$ for electrons and i for ions. Δn and l_0 gives the amplitude and width of the superimposed density perturbation. Here, x_c is the center of simulation system, i.e., $L_x/2$. The initial density perturbation (IDP) is purposely introduced away from the center of the simulation system by taking $\alpha = -L_x/4$, so that the IASWs generated in the system can counter propagate and collide with each other. We take 50 000 superparticles per grid dx, which corresponds to a total number of 2×10^9 superparticles for each species. The idea of using a large number of particles is to reduce thermal fluctuations in the simulation system. We consider the initial density perturbation with $\Delta n = 0.5$ and $l_0 = 102$. Based on Kakad et al.,[7,30] the IDP falls in the long wavelength regime ($k^2 \lambda_{de}^2 < 1$) and it is demonstrated that such IDP is more likely to be evolved into multiple IASWs in the plasmas through the process of wave breaking.[7,30]

We perform the simulation of plasma with no magnetic field. The perturbation applied to such plasma creates charge separation that arises the finite electric field in the system. This electric field then drives two electrostatic normal modes, namely, a high and a low frequency mode. The high-frequency mode is the Langmuir wave in which the electrons oscillate rapidly about stationary ions, and the low-frequency waves are the ion acoustic waves that are generated through longitudinal oscillation of the ions in a plasma. The generation and evolution of multiple counter-propagating IASWs

driven by the IDP in electron and ion equilibrium densities are shown in Fig. 1. The panels in first and second rows of this figure, respectively, show electron and ion phase space distributions at the different timings, $\omega_{pi}t = 0$, 34, 57, 250, 300, and 360. The panels in third and fourth rows, respectively, show the evolution of particle densities and electrostatic potential in the system at corresponding times. The panels at $\omega_{pi}t = 0$ show the initial setup of the simulation, when IDP is introduced in uniformly distributed superparticles. At this stage, the injection of the IDP causes charge separation in the plasma that setup an infinitesimal electrostatic potential in the system, which grows with time. This potential pulse then evolves into two oppositely propagating IASW pulses. One of the snapshots of such pulses is shown at $\omega_{pi}t = 34$. Ions play an important role in the generation of these waves. One can see two local enhancements in ion and electron densities linked with the two IASWs that are propagating in opposite direction (supplementary material).

Simulation shows that the low energy electrons are trapped into the counter-propagating positive wave potentials forming electron vortices in the phase space distribution of the electrons. The trapped electrons involve electrons resonating with the potential well of the IASWs and accompanying it in their propagation. They appear as a hump in the phase space as described by Schamel.[31] The ions are also found to respond as per the direction of the motion of trapped electrons in the wave potential. As a result, one hump and one dip are seen in the ion phase space distribution. In the course of the propagation of the IASW pulses toward the simulation boundaries, both pulses acquire critical amplitude through steepening and then break. The snapshots of the phase space distributions and densities of the electrons and ions, and the electrostatic potential at the time of the initiation of the
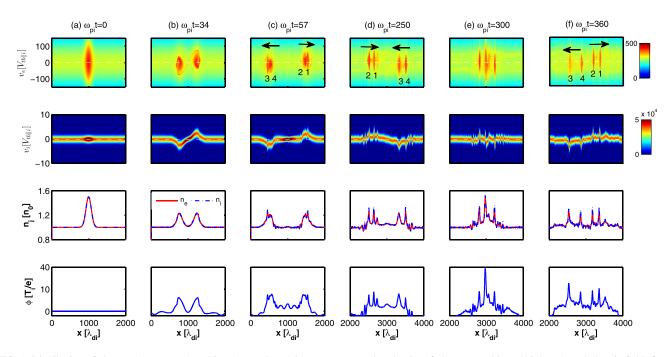

FIG. 1. Distribution of electrons (upper row) and ions (second row) in x–v space, number density of electrons and ions (third row), and electric field (fourth row) as a function of x at (a) initial time $\omega_{pi}t = 0$, (b) formation of two counter-propagating IASWs at $\omega_{pi}t = 34$, (c) trapped electron vortices linked with IASWs starts breaking at $\omega_{pi}t = 57$, (d) two counter-propagating pairs of IASWs are formed through wave breaking at $\omega_{pi}t = 250$, (e) IASWs collide with each other at $\omega_{pi}t = 300$, and (f) vortices of trapped electrons linked with IASWs emerge out from each other after collision at $\omega_{pi}t = 360$.

breaking of the IASW (i.e., $\omega_{pi}t = 57$) are shown in Fig. 1.
Later, each of these pulses breaks into two IASW pulses to
form two oppositely propagating chains of IASW pulses. At
the breaking of the IASW pulse, each of the electron vortex,
and the ions hump in their respective phase space distribu-
tions also splits into two. The leading and following vortices
of trapped electrons associated with IASWs propagating
towards rightside and leftside boundaries of the simulation
system are, respectively, marked as 1, 2 and 3, 4, in Fig. 1. It
is noticed that the amplitudes of the leading IASWs are rela-
tively smaller than the subsequent IASWs. After sufficient
time, these IASW structures detached from each other
because of difference in their phase speeds. Subsequently,
two chains of counter-propagating IASWs are formed in the
system. The IASWs in both oppositely propagating chains
are distinguishable and they are nearly stable during their
propagation.

   In the periodic system, the IASW pulse/vortices propa-
gating on the left side reaches the boundary early, and then
enters through the right sight-side boundary of the system.
One of the snapshots of the IASW pulse/vortices during such
propagation is shown in Fig. 1(d) at $\omega_{pi}t = 250$. It is observed
that the counter-propagating ion acoustic (IA) pulses/vortices
collide with each other after few time steps. One of the snap-
shots of these IA pulses/vortices in the course of collision is
shown at $\omega_{pi}t = 300$ in Fig. 1(e). At this time, the two fore-
most counter-propagating IASW pulses/vortices are collided,
which later come out of each other without much losing their
characteristics. These pulses/vortices then again collide with
other incoming pulses/vortices and came out through each
other without much change in their characteristics. This prop-
erty of the IASW pulses shows a behaviour of solitons, as
their width, amplitude, and the speed of these IASWs remain
relatively unchanged after their mutual interaction. One of
the snapshots of the phase space distributions, densities of the
electrons and ions, and electrostatic potential of the IASWs
coming out of each other after their head-on collision is

shown in Fig. 1(f) at $\omega_{pi}t = 360$. The reason behind sustaining
the original characteristics of the IASWs after their multiple
collisions is related to the local ion dynamics at the IASW
pulses. We observed electron vortices in the electron phase
space, while humps and dips in the ion phase space associated
with the IASW pulses. At the time of the interaction of
IASW pulses, the humps and dips in the ion phase space are
superimposed in space, but they are separated in velocity.
Therefore, they come out of each other without much change
in their characteristics. The electron vortices nonlinearly
interact with each other and they emerged out of each other
without much change, because wave potentials are deter-
mined by the dynamics of ions.

   We examined the spatio-temporal variation of the elec-
tron and ion densities associated with the IASWs, which is
shown in Figs. 2(a) and 2(b), respectively. The yellow bands
in these figures represent the densities associated with the
IASW structures. It is seen that the IDP initially evolved into
two oppositely propagating IASW pulses. Later, each of
these IASW pulses break into the two distinguishable (slow
and fast) IASW pulses. The IASW pulses propagating in
the negative x-direction reaches to the left boundary of the
simulation system and then they renter the system through
the right-side boundary of the simulation system due to the
periodic boundary conditions. In this way, the counter-
propagating IASWs in both chains come closer and collide
with each other during $\omega_{pi}t = 280$–325. After their head-on
collisions, the IASW pulses come out of each other. Before
the multiple collisions, the IASWs propagating towards
right-side (left-side) boundary of the simulation system are
having phase speeds $13.14V_{t\|i}$ and $12.28V_{t\|i}$ ($13.96V_{t\|i}$ and
$12.10V_{t\|i}$) for the pulses 1 and 2 (3 and 4), respectively, as
marked in Fig. 1(d). After the multiple collisions, the phase
velocities of the IASWs are found to increase slightly. The
phase velocities (V_s) of the IASW pulses travelling towards
the right-side (left-side) simulation boundary are $13.42V_{t\|i}$
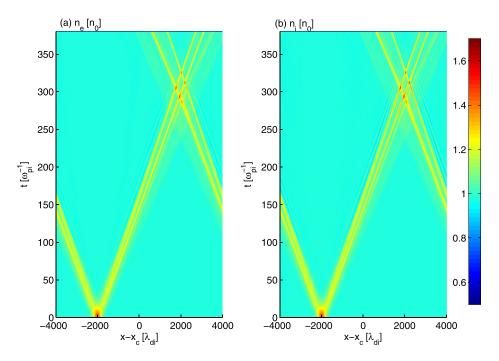and $13.0V_{t\|i}$ ($14.14V_{t\|i}$ and $12.58V_{t\|i}$). This indicates the

FIG. 2. Spatio-temporal evolution of
the densities of the electrons and ions
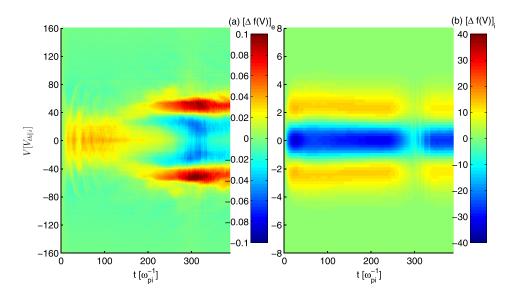in the simulation.

FIG. 3. Time evolution of change in distribution function as compared to its initial distribution (i.e., $[\Delta f(V)]_j$) for (a) electrons and (b) ions.

phase shift during interaction of the multiple counter-propagating IASW pulses. From Fig. 2, it is observed that the velocity of each IASW pulse increased when it approaches and collides with another pulse coming from opposite direction. This advancement in phase happens twice as each pulse interacts with two IASW pulses coming from the other direction. The amount of change in the phase for the slower pulse is found to be large as compared to that for the faster pulse. These phase shift characteristics are consistent with the previous studies.[15,21,32]

In our simulation, the IASW characteristics before and after the collisions are comparable, and their collisions are quasi-elastic. At the time of collision, the forward and backward propagating trapped electrons are strongly affected by a locally modified potential because of their short trapping period. However, the forward and backward propagating ions in the phase space do not undergo much change because they have larger momentum and the larger trapping period as compared to that of electrons. Thus, the dynamical characteristics of forward and backward propagating ion populations are less significantly affected by the IASW collisions. As a result, the collision of IASWs is found to be quasi-elastic.

We investigated the particle acceleration in the process of the head-on collision of these counter-propagating IASWs. For this purpose, we examine time variation of the distribution functions for ions and electrons. The initial distribution function at $\omega_{pi}t = 0$ is subtracted from the distribution function at a given time $\omega_{pi}t$ for each species to obtain the variation in the distribution function, i.e., $[\Delta f(V)]_j$. The time evolution of variation of the distribution functions for electrons and ions is presented in Figs. 3(a) and 3(b), respectively. It is seen from Fig. 3(a) that the lower thermal velocity electrons (10–$30V_{t\|i}$) trapped within both forward and backward propagating phase-space vortices are accelerated to higher velocities (40–$60V_{t\|i}$) during the head-on collisions of counter-propagating IASWs. However, Fig. 3(b) shows slight deceleration of the higher velocity ions during the collisions of IASWs.

We have examined the evolution of electrostatic energy, and kinetic energy of the electrons and ions for the simulation

run discussed here. For this purpose, the energies at $\omega_{pi}t = 0$ are subtracted from the corresponding estimates of electrostatic and kinetic energies at other time to obtain the change in these energies. Figures 4(a), 4(b), and 4(c), respectively, show the time variation of change in electrostatic energy (ΔE_s), electron kinetic energy (ΔKE_e), and ion kinetic energy (ΔKE_i). It is seen that the electrostatic energy increases at the time of collision of the IASWs with other IASWs in the system. The variation in the maximum kinetic energy of the electrons given in Fig. 4(b) shows that the electrons gain kinetic energy during interaction of the counter-propagating IASW phase space structures. At the same time, it is seen that the maximum kinetic energy of the ions decreases during collision of the counter-propagating IASW phase space structures, which is displayed in Fig. 4(c). This indicates that the electrons (ions) are accelerated (decelerated) locally at the time of collision of the counter-propagating IASWs. Furthermore, the total kinetic energy in the system (i.e., the sum of kinetic energy of electrons and ions) before and after collision is
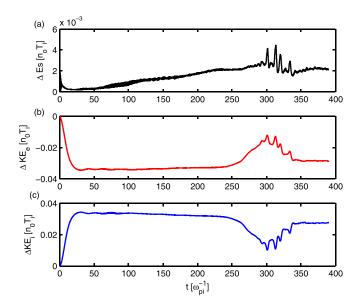

FIG. 4. Evolution of change in (a) electrostatic energy, (b) electron kinetic energy, and (c) ion kinetic energy as a function of time.

nearly the same. This hints again the quasi-elastic interaction of counter-prorogating IASWs in the present plasma simulation. To summarize, the formation and interaction of the multiple IASWs have been observed in a plasma through PIC simulation. The long wavelength perturbation is used to excite the multiple counter-propagating IASWs in the system. The evolutionary process of the formation of multiple IASWs can be understood in two steps. In the early phase, the stationary IDP evolves into two oppositely propagating IASWs along with the Langmuir mode. These IASWs are indistinguishable and their velocities are self-consistent. At later stage, each of the moving IASWs starts to steepen due to the increase in nonlinear effects, and then evolved into two IASW pulses through wave breaking. The breaking of the IASWs is similar to those reported by Jenab and Spanier[33] by using Vlasov simulations.

In the simulation, the counter-propagating IASWs are allowed to interact with each other under the periodic boundary conditions. The four counter-propagating IASWs with different amplitudes and widths are found to survive after head-on collisions between them, which suggests that the observed solitary waves follow soliton type characteristics. Also, it is observed that the kinetic energy and the IASW characteristics before and after collision in the system are comparable.

In conclusion of this paper, the head-on collision of counter-propagating IASWs is found to be quasi-elastic in nature. It is also found that the thermal electrons trapped in the potentials of the IASWs are accelerated to higher velocities, resulting in the increase of kinetic energy of the electrons during the process of head-on collisions of the multiple IASWs in the system. The local plasma parameters in space plasmas support a variety of solitary wave structures with different characteristics. Thus, the existence of local electron acceleration by mutual interaction of multiple solitary waves with each other is relevant for space plasmas, including planetary magnetospheres.

See supplementary material for the animation of the head-on collision of multiple counter-propagating coherent phase space structures associated with the IASWs in a plasma.

[1]H. Matsumoto, H. Kojima, T. Miyatake, Y. Omura, M. Okada, I. Nagano, and M. Tsutsui, Geophys. Res. Lett. **21**, 2915, doi:10.1029/94GL01284 (1994).

[2]J. Pickett, S. Kahler, L.-J. Chen, R. Huff, O. Santolik, Y. Khotyaintsev, P. Décréau, D. Winningham, R. Frahm, M. Goldstein *et al.*, Nonlinear Processes Geophys. **11**, 183 (2004).

[3]G. Lakhina, S. Singh, A. Kakad, M. Goldstein, A. Vinas, and J. Pickett, J. Geophys. Res.: Space Phys. **114**, A09212, doi:10.1029/2009JA014306 (2009).

[4]G. Lakhina, S. Singh, A. Kakad, and J. Pickett, J. Geophys. Res.: Space Phys. **116**, A10218, doi:10.1029/2011JA016700 (2011).

[5]A. Kakad, B. Kakad, C. Anekallu, G. Lakhina, Y. Omura, and A. Fazakerley, J. Geophys. Res.: Space Phys. **121**, 4452, doi:10.1002/2016JA022365 (2016).

[6]B. Kakad, A. Kakad, and Y. Omura, J. Geophys. Res.: Space Phys. **119**, 5589, doi:10.1002/2014JA019798 (2014).

[7]A. Kakad, Y. Omura, and B. Kakad, Phys. Plasmas **20**, 062103 (2013).

[8]A. Lotekar, A. Kakad, and B. Kakad, Phys. Plasmas **23**, 102108 (2016).

[9]A. Kakad, A. Lotekar, and B. Kakad, Phys. Plasmas **23**, 110702 (2016).

[10]G. Lakhina, A. Kakad, S. Singh, and F. Verheest, Phys. Plasmas **15**, 062903 (2008).

[11]G. S. Lakhina, S. Singh, and A. Kakad, Adv. Space Res. **47**, 1558 (2011).

[12]S. Sharma, A. Boruah, and H. Bailung, Phys. Rev. E **89**, 013110 (2014).

[13]S. Jaiswal, P. Bandyopadhyay, and A. Sen, Phys. Plasmas **21**, 053701 (2014).

[14]S. K. Sharma, A. Boruah, Y. Nakamura, and H. Bailung, Phys. Plasmas **23**, 053702 (2016).

[15]X. Qi, Y.-X. Xu, W.-S. Duan, L.-Y. Zhang, and L. Yang, Phys. Plasmas **21**, 082118 (2014).

[16]S. El-Tantawy, W. Moslem, R. Sabry, S. El-Labany, M. El-Metwally, and R. Schlickeiser, Astrophys. Space Sci. **350**, 175 (2014).

[17]F. Verheest, M. A. Hellberg, and W. A. Hereman, Phys. Rev. E **86**, 036402 (2012).

[18]P. Carbonaro, Eur. Phys. J. D **66**, 302 (2012).

[19]F. Verheest, M. A. Hellberg, and W. A. Hereman, Phys. Plasmas **19**, 092302 (2012).

[20]N. Saini and K. Singh, Phys. Plasmas **23**, 103701 (2016).

[21]D. Mandal and D. Sharma, Phys. Plasmas **23**, 022108 (2016).

[22]S. El-Tantawy and W. Moslem, Phys. Plasmas **21**, 052112 (2014).

[23]S. El-Tantawy, A. Wazwaz, and R. Schlickeiser, Plasma Phys. Controlled Fusion **57**, 125012 (2015).

[24]S. El-Tantawy, Chaos, Solitons Fractals **93**, 162 (2016).

[25]S. Hosseini Jenab and F. Spanier, Phys. Plasmas **24**, 032305 (2017).

[26]K. Roy, M. K. Ghorui, P. Chatterjee, and M. Tribeche, Commun. Theor. Phys. **65**, 237 (2016).

[27]Y. Omura and H. Matsumoto, Comput. Space Plasma Phys.: Simul. Tech. Software **21**, 21 (1993).

[28]Y. Omura, H. Kojima, and H. Matsumoto, Geophys. Res. Lett. **21**, 2923, doi:10.1029/94GL01605 (1994).

[29]Y. Omura, in *Advanced Methods for Space Simulations*, edited by H. Usui and Y. Omura (Terra Science, Tokyo, 2007), p. 1.

[30]A. Kakad and B. Kakad, Phys. Plasmas **23**, 122101 (2016).

[31]H. Schamel, Plasma Phys. **14**, 905 (1972).

[32]T. Tsuboi, Phys. Rev. A **40**, 2753 (1989).

[33]S. Hosseini Jenab and F. Spanier, Phys. Plasmas **23**, 102306 (2016).